View metadata, citation and similar papers at core.ac.uk
brought to you by CORE
provided by Elsevier - Publisher Connector

Elucidating the medium-resolution structure of ribosomal particles: an interplay between electron cryo-microscopy and X-ray crystallography

Jörg Harms[1‡], Ante Tocilj[2‡], Inna Levin[2‡], Ilana Agmon[2‡], Holger Stark[3†‡], Ingo Kölln[1], Marin van Heel[3], Marianne Cuff[3], Frank Schlünzen[1], Anat Bashan[2], Francois Franceschi[4] and Ada Yonath[1,2*]

Background: Ribosomes are the universal cellular organelles that accomplish the translation of the genetic code into proteins. Electron cryo-microscopy (cryo-EM) has yielded fairly detailed three-dimensional reconstructions of ribosomes. These were used to assist in the determination of higher resolution structures by X-ray crystallography.

Results: Molecular replacement studies using cryo-EM reconstructions provided feasible packing schemes for crystals of ribosomes and their two subunits from *Thermus thermophilus*, and of the large subunits from *Haloarcula marismortui*. For the large subunits, these studies also confirmed the major heavy-atom sites obtained by single isomorphous replacement combined with anomalous diffraction (SIRAS) and by multiple isomorphous replacement combined with anomalous diffraction (MIRAS) at ~10 Å. Although adequate starting phases could not be obtained for the small subunits, the crystals of which diffract to 3.0 Å, cryo-EM reconstructions were indispensable for analyzing their 7.2 Å multiple isomorphous replacement (MIR) map. This work indicated that the conformation of the crystallized small subunits resembles that seen within the 70S ribosomes. Subsequently, crystals of particles trapped in their functionally active state were grown.

Conclusions: Single-particle cryo-EM can contribute to the progress of crystallography of non-symmetrical, large and flexible macromolecular assemblies. Besides confirming heavy-atom sites, obtained from flat or overcrowded difference Patterson maps, the cryo-EM reconstructions assisted in elucidating packing arrangements. They also provided tools for the identification of the conformation within the crystals and for the estimation of the level of inherent non-isomorphism.

Addresses: [1]Max-Planck Research Unit for Ribosomal Structure, Notke Strasse 85, 22603 Hamburg, Germany, [2]Department of Structural Biology, Weizmann Institute, 76100 Rehovot, Israel, [3]Imperial College of Science, Technology and Medicine, Department of Biochemistry, London SW7 2AY, UK and [4]Max-Planck Institute for Molecular Genetics, Ihnestrasse 73, 14195 Berlin, Germany.

[†]Present address: Marburg University, Institute for Molecular Biology & Cancer Research, Marburg, 35037, Germany.

*Corresponding author.
E-mail: YONATH@mpgars.desy.de

[‡]These authors made a major contribution to these studies.

Key words: electron cryo-microscopy, MIR phasing, MR searches, ribosomes

Received: 14 October 1998
Revisions requested: 4 December 1998
Revisions received: 3 March 1999
Accepted: 21 April 1999

Published: 15 July 1999

Structure August 1999, 7:931–941
http://biomednet.com/elecref/0969212600700931

© Elsevier Science Ltd ISSN 0969-2126

Introduction

Ribosomes, discovered in the mid-fifties, are the universal cellular organelles on which the sequential polymerization of amino acids according to the genetic code takes place. They are giant ribonucleoprotein assemblies (called 70S in bacteria), consisting of two subunits of unequal size (called 50S and 30S in bacteria) that associate upon initiation of protein biosynthesis. Extensive efforts have been made to elucidate the three-dimensional structure of the ribosome, using a large range of techniques including X-ray crystallography and advanced cryo-electron microscopy (cryo-EM).

We have grown two types of three-dimensional crystals of ribosomal particles that diffract to around 3 Å resolution: those of the large subunits from *Haloarcula marismortui*, H50S, and those of the small subunits from *Thermus thermophilus*, T30S [1,2]. Difficulties in carrying out crystallographic analysis of them reflect their unfavorable characteristics. Not only are the ribosomes of a huge size with no internal symmetry, they also exhibit internal flexibility and have a surface that is rich in readily degradable RNA and loosely attached proteins. Moreover, most of the ribosomal crystals show extreme radiation sensitivity, poor isomorphism and non-isotropic mosaicity. They yield deformed spot shapes and suffer from an increase in the unit-cell dimensions during X-ray exposure.

Electron microscopy of ribosomal particles has undergone significant developments over the past few years. The introduction of single-particle cryo-EM, in combination with powerful computational procedures such as angular reconstitution [3–6], has yielded detailed three-dimensional

images of bacterial ribosomal particles and their functional complexes [7–13]. These three-dimensional reconstructions resemble the consensus topography observed by traditional negative-staining EM and confirm the existence of internal features, mainly associated with vacant spaces such as tunnels and hollows, detected about a decade ago in reconstructions from negatively stained crystalline arrays [14–17]. They have also been interpreted along similar lines, in conjunction with biochemical findings accumulated over three decades [18,19]. Using the reconstructions obtained from negatively stained arrays we have conducted combined EM/X-ray studies at different levels [20] that clearly pointed to the need for more detailed starting models.

With the availability of cryo-EM three-dimensional reconstructions, a fruitful interface between EM imaging and X-ray crystallography became feasible. The suitability of EM information for yielding adequate X-ray phases that lead to structure determination was first shown for the tomato bushy stunt virus, a system with a high level of noncrystallographic symmetry [21]. Similar studies were performed later on other viruses [22] and smaller macromolecules [23]. In studies of complicated structures, such as the proteosome [24] and the chaperonin GroEL [25], EM was useful in confirming their internal symmetry. The overall shape of the nucleosome [26], as observed by EM, was initially combined with the known DNA periodicity. EM of muscle fibers and high-resolution structures of the muscle proteins were exploited together for the determination of the structure of the actin–myosin complex [27]. Only a few molecular replacement (MR) studies of large assemblies with no internal symmetry, such as ribosomes, however, have been reported so far [2,19,28].

We report here three approaches to MR studies of ribosomal particles from *T. thermophilus* and of H50S, the large ribosomal subunit from *H. marismortui*. We used pure MR searches and their verification by noncrystallographic information for the 70S ribosomes from *T. thermophilus*, T70S. We then employed MR combined with experimental phasing, including the confirmation of heavy-atom sites detected independently by crystallographic methods, for the 50S subunits from *T. thermophilus*, T50S, and for H50S. For the latter, the exploitation of the MR results for the estimation of the level of non-isomorphism and the suitability of the crystallographic data for efficient phasing is suggested. We employed MR as a tool for confirming independently determined packing diagrams, for better understanding of crystal selectivity and for the design of controlled conformational rearrangements within the crystals for T30S.

Results

The whole ribosome: T70S

The T70S reconstruction, performed at 24 Å resolution as for E70S (70S from *Escherichia coli*) [7,8], revealed detail including a network of tunnels through the 50S part and a large gap between the two subunits, similar to features detected earlier in reconstructions from two-dimensional arrays of 50S and 70S from *Bacillus stearothermophilus* [15,16]. T70S crystals diffract to a comparable resolution, 20–24 Å [29–31]. A complex of T70S with two molecules of PhetRNA^{Phe}, however, yielded crystals isomorphous to those of T70S but diffracting to 12–17 Å [31]; the latter were used for the MR studies.

A unique solution, with Cf (correlation coefficient, calculated using structure factors) of 72%, Ci (correlation coefficient, calculated using intensities) of 73%, agreement factor (R) of 45% and a contrast (the ratio between the correlation coefficient of the best solution and that of the following one) of 1.5, was obtained when the EM reconstruction was expanded isotropically by 2% (see Materials and methods section) and used for MR searches at 20–40 Å (Figure 1). The same solution was obtained for a large range of resolutions and radii, but with somewhat inferior scores. The map assembled according to this solution (Figure 2) shows no collisions or short contacts, and the MR packing scheme agrees with the arrangement detected in electron micrographs of positively stained thin sections of the T70S crystals.

The large ribosomal subunits: T50S and H50S

The crystals of T50S diffract nominally to 8.7 Å [32], but yield useful data to only 10–12 Å. Rotation and translation searches were performed using the 17 Å cryo-EM reconstruction of this particle, shrunk isotropically by 4% (see Materials and methods section). These searches (Figure 3) resulted in a single unique solution (Cf = 65%, Ci = 67%,

Figure 1

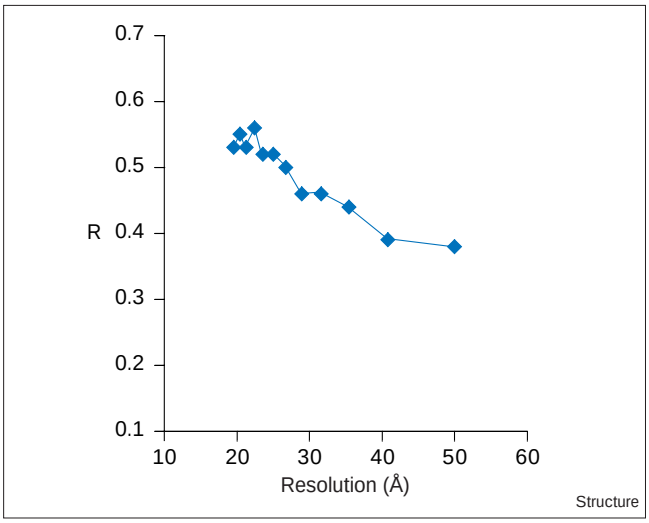

The agreement factor R(F_c/F_{obs}) of the MR result for the cryo-EM reconstruction of T70S in the crystal, as a function of resolution.

Figure 2

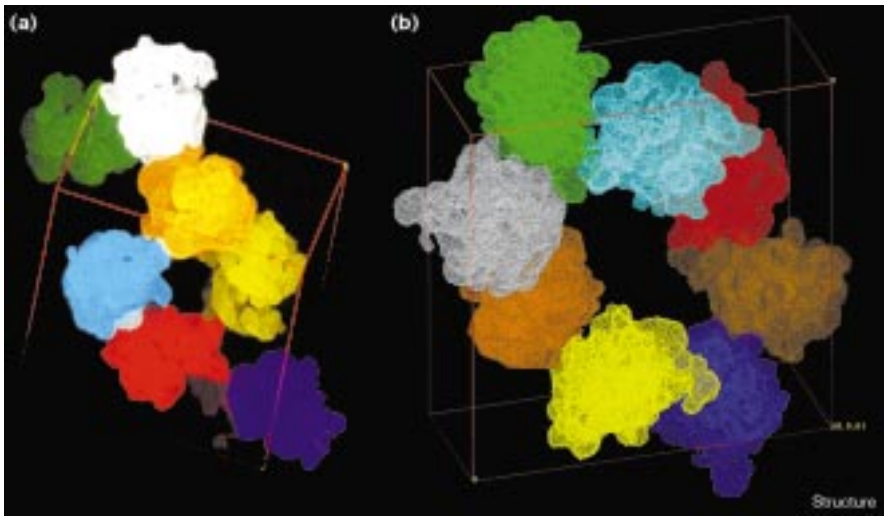

(a) The packing of the whole ribosome (T70S), assembled by positioning the 24 Å EM reconstruction in the crystallographic unit cell according to the MR search. (b) The packing of the large ribosomal subunit (T50S), assembled by positioning the 17 Å EM reconstruction in the crystallographic unit cell according to the MR results.

R = 41% and contrast(i) = 1.8) exhibiting normal interparticle contacts without overlap (Figure 2).

Crystallographic data were collected to 10 Å from native and Ta_6Br_{14}-soaked crystals of T50S. Two sites, extracted from isomorphous and anomalous difference Patterson maps, were used for initial SIRAS (single isomorphous replacement combined with anomalous diffraction). Final statistics: R_{cullis} = 0.59 (total); 0.87 (anomalous); phasing power = 1.95; figure of merit (FOM) = 0.58. These two sites were placed in the map phased according to the MR results and found to be in crystallographically sound positions [2,19]. Half a dozen sites with heights of around 4σ were detected in a difference Fourier map on the basis of the MR phases, and one corresponds to the main Ta_6Br_{14} SIRAS site. These sites might be used for extending the detail of the cryo-EM reconstruction, from its original 17 Å to the crystallographic limit of 10 Å resolution (work in progress).

Although the crystals of H50S diffract to the highest resolution obtained for ribosomal particles, 2.7 Å, they possess several undesirable properties that become less tolerable with the increase of resolution, among them a severe sensitivity to X-ray irradiation coupled with an extremely low level of isomorphism. Hence, their structure determination is performed in stages from lower to higher resolution. The shape of the particle as observed in the 12 Å MIRAS (multiple isomorphous replacement combined with anomalous diffraction) map [2], currently extended to 7.5 Å, is similar to that obtained by cryo-EM for large subunits from various bacterial sources [2,7,8,15,19,33]. It shows gross features that were identified by EM at lower resolution, such as the exit tunnel, but in more detail. It also contains elongated dense regions, interpretable as single- and double-stranded RNA chains.

The packing arrangement of these crystals is such that H50S particles form two closely packed layers, connected by a narrow contact region in the middle of the c axis (Figure 4). This contact area is surrounded by a very large continuous solvent region, reaching dimensions of more than 240 × 140 × 100 Å. The limited size of the interparticle contact region permits only a small number of interactions. This might cause the poor isomorphism, the unfavorable crystal habit (plates, made of sliding layers, reaching typically up to 0.5 mm^2 with an average thickness of a few microns in the direction of the c axis), and the variations in the c axis length (567–570 Å) as a function of irradiation [2].

The native data set used for MIRAS phasing was exploited for MR validation tests in order to minimize the probability of bias originating from the low level of isomorphism. A satisfactory packing arrangement was

Figure 3

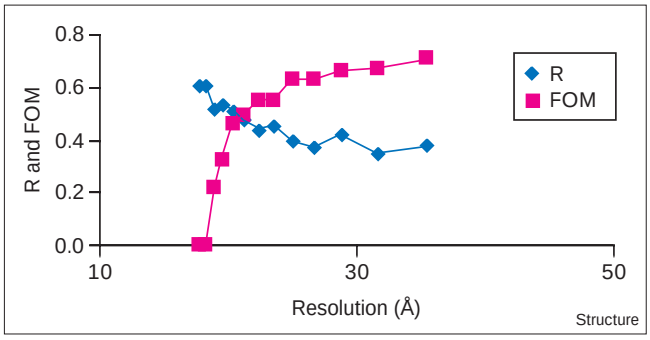

The agreement factor $R(F_c/F_{obs})$ and the figure of merit (FOM) values obtained for the MR result for the packing diagram of the crystals of T50S, as a function of resolution.

Figure 4

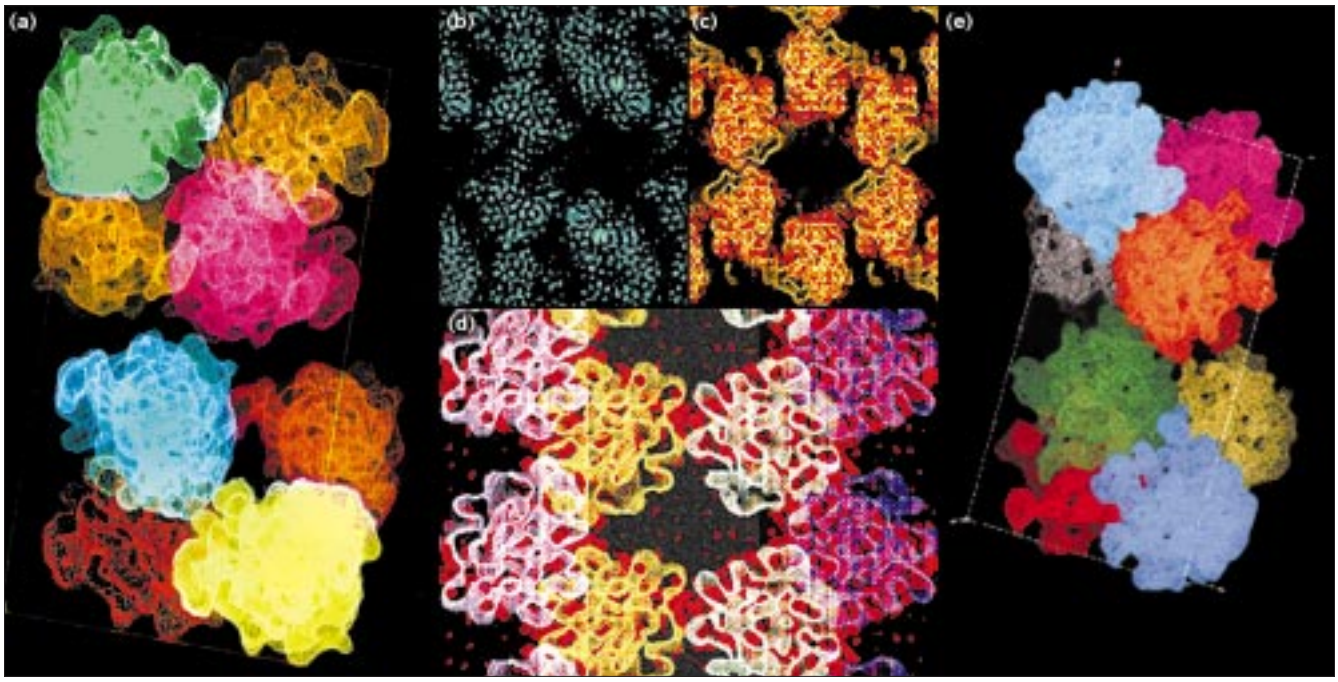

The packing arrangement of H50S crystals. **(a)** The MIRAS compatible MR packing arrangement of H50S crystals. **(b)** A slice of about 20 Å thickness of the H50S MIRAS map, showing the loose contact and the site of the main heavy atom. **(c,d)** Two slices, each of about 40 Å thickness, of the MR solution overlaid on the MIRAS map (shown in red), highlighting the main difference between the results of the two methods. **(e)** For comparison, the result of the parallel MR studies (this figure was reproduced from [28] with permission).

obtained (93% correlation, R factor 27% for 60–90 Å and 39–50% correlation with R factor 42–47% for 30–95 Å), showing the packing observed in the MIRAS map (Figure 4). For confirming the previously determined major site of Ta_6Br_{14}, the strongest H50S derivative [32], we first established that it is detectable in difference Patterson maps constructed at lower than 17 Å, the limit dictated by the cryo-EM reconstruction.

It should be mentioned that the salts required for functional activity of H50S (2.5–3 M KCl and 0.5 M NH_4Cl) hamper cryo-EM studies. The only available EM reconstruction of H50S was obtained using a solution of significantly lower salt concentration [28], close to that used at the initial step of H50S crystallization [1,34]. We used this low salt concentration to control the crystallization process because the crystallization terminated after a few hours in a shower of disordered microcrystals when the higher salt concentration necessary for activity was employed. Hence, we designed a procedure in which crystallization occurs in solutions with the minimum salt needed for the integrity of the particle (1.2–1.7 M KCl and 0.5 M NH_4Cl), at which no functional activity was detected. Once the crystals are formed they are transferred to solutions containing the salts required for functional activity [18,34], allowing X-ray measurements under these conditions.

We used the higher resolution cryo-EM reconstruction of T50S (17 Å) for MR searches of the H50S crystals because we believed that the similarity between the active conformations of 50S in the two bacteria should be a better basis for MR searches than the similarity between active and inactive conformations from the same bacterium. This assumption was confirmed in our studies as well as studies from another group using data from crystals of H50S grown under the same crystallization conditions and an EM reconstruction of the large subunit cut from that of 70S from *E. coli* [28].

Thus, it seems that the gross conformations of the large ribosomal subunits from archea and eubacteria are rather similar, and that this similarity is maintained even in slightly different environments, as long as the integrity of the particles is not harmed. The differences among the species, however, are not negligible. Indications for them were detected even at very low resolution, as seen by the decrease in the scores with progression from 60–30 Å.

Comparison of the MIRAS and the MR maps at comparable resolution (Figure 4) showed the same packing arrangements with the same positions of the centers of mass (COM) of the particles. The main differences between the MIRAS and MR maps are in the locations assigned to L1

and L7 proteins by EM. These two proteins are well resolved in the cryo-EM reconstructions, but diffuse into the solvent in the MIRAS map (Figure 4), probably because of the similarity in the electron density of the solution within the H50S crystals (3 M KCl) and that of proteins [2].

Similarities were detected between the MR packing arrangement and that revealed by neutron diffraction [35]. In addition, the MR-determined COMs of H50S as determined elsewhere at comparable resolution [28] are located at approximately the same position as in our studies, but with different orientation (Figure 4). This suggests a link between the variations in the orientations of the particles and the level of non-isomorphism. We therefore examined the MR solutions obtained for over two dozen H50S data sets of native, derivatized and chemically treated particles. We found that some of the data sets led to solutions with reasonable scores that fall into the category described above: similar COM positions, but variability in the orientations. Other data sets led to several unrelated solutions. The classification by COM provided a tool to discriminate between extreme and moderate deviations from isomorphism and assist in the selection of consistent data sets for MIR phasing. This approach might be unnecessary in standard cases, but it should be increasingly useful for studies of giant macromolecular complexes that yield overcrowded, flat and difficult to interpret difference Patterson maps.

The resolution of the crystallographic studies of H50S is currently being significantly extended, as a 5 Å anomalous data set of the Ta_6Br_{14} derivative gave difference Patterson maps that show a major site consistent with our lower resolution results [2]. Hence we have decided to delay the interpretation until a later stage.

The small ribosomal subunit: T30S

In contrast to the impressive progress in image reconstruction of 70S ribosomes and 50S subunits, until recently the small ribosomal subunit was reconstructed to only 37 Å resolution [36]. The flexibility and instability of the small subunits is easily demonstrated. Exposure of 70S ribosomes to proteolytic enzymes resulted in complete digestion of the 30S subunits and left the 50S subunits essentially intact. Furthermore, crystallization attempts with functionally active 70S ribosomes that were formed from *in vitro* associated subunits, yielded crystals of the 50S subunits and degradation of the 30S [18,37]. For our cryo-EM reconstructions, therefore, we used the preparations that yielded the best three-dimensional crystals. Nevertheless, these yielded reconstructions at only 25 Å (Figure 5), a resolution limit that is significantly poorer than that obtained for T50S, but the highest obtained from 30S to date.

The two crystal forms of T30S that we obtained are clearly non-isomorphous (R scale above 60%), even though their unit-cell parameters are virtually identical ($P4_12_12$, a = b = 405 Å, c = 176 Å). The first crystal form (called T30S-LR) was characterized about ten years ago [38], but was not extensively studied because its diffraction yielded useful data to only 12–18 Å [39]. Subtle modifications in the procedures of bacterial growth and crystal treatment recently led to a higher resolution, 3.0 Å. The current MIR 7.2 Å electron-density map of these crystals (called T30S-HR) reveals elongated dense regions similar to those detected in the nucleosome at comparable resolution levels [40] and globular or elliptic lower resolution regions, appropriate to host ribosomal proteins.

Among the main features of the 7.2 Å map are extensive pairing of the particles and an internal continuous solvent region of a fairly large size, both detected earlier by conventional negative-stain EM. The large solvent region was first observed in EM studies of positively stained thin sections of epon-embedded T30S-LR crystals (Figure 6). The pairing contacts are extremely stable and maintained even after the rest of the crystal network is destroyed. Thus, EM of dissolved T30S-HR crystals showed the majority of the particles as pairs with a typical butterfly-like shape (Figure 6), similar to the organization in the crystal (Figure 7). These two prominent features were also

Figure 5

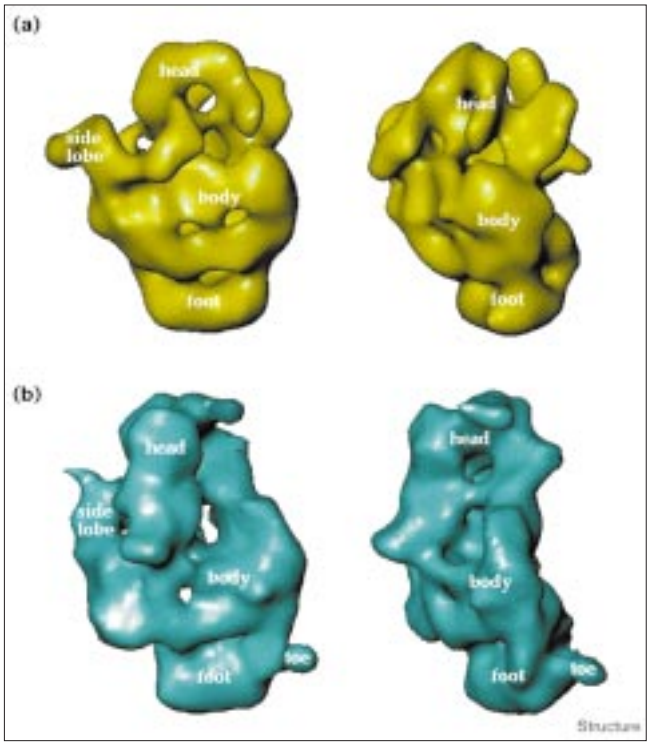

(a) Two views of the 25 Å cryo-EM reconstruction of the isolated (free) T30S. (b) The bound form of T30S (the cut model, obtained by removing the density assigned for T50S in the reconstruction of T70S), positioned in the same orientation as (a).

observed in the MR packing diagrams of T30S-LR and T30S-HR crystals, using the reconstructions of free T30S (Figure 6). Despite the difference in scores obtained from MR searches of T30S-LR (Cf = 66.0%, R = 46.4%, contrast(f) = 1.2) and of T30S-HR (Cf = 40.2%, R = 54.5%, contrast(f) = 1.1), at a first glance the two solutions show a high degree of similarity. Indeed, the COM's of the particles are almost identical but their relative orientations differ by approximately 80°. Thus, in the HR crystals the upper part of T30S (called the head, and known to be flexible) is involved in extensive contacts, whereas in the LR form it points into the solution. It is conceivable that free movement of the heads allowed by the LR packing arrangement causes the lower resolution of this crystal form. Hindrance of these movements by the crystal network might be the reason for the higher order of the T30S-HR crystals.

Attempts to fit the contour of the cryo-EM three-dimensional reconstruction of the free 30S particle onto the MIR map met with some difficulties, because the cryo-EM and the X-ray map are different in length-to-width ratio as well as in various finer details (Figure 7). Careful inspection of the MIR map indicates, however, that the crystallized particles have a conformation similar to that of the small subunit when bound to the 50S within the 70S ribosome. To further assess this point, we computed the reconstruction of a 'bound' T30S by removing the density that was originally assigned to the 50S subunit within the three-dimensional reconstruction of the T70S ribosome (Figure 5). This reconstruction, called here the 'cut' T30S, led to a reasonable agreement with the main features of the 7.2 Å MIR map (Figure 7). Indeed, using the data from the HR crystals, MR searches gave rise to a solution with reasonable scores (Cf = 52.2, R = 44.8, 40–80 Å) and an arrangement grossly fitting the MIR packing diagram. This arrangement, however, suffers from moderate interparticle collisions, presumably because the cut three-dimensional reconstruction does not provide an accurate representation of the conformation selected by the HR crystals.

The fitting experiments suggested that a part of the pairing contacts within the crystals utilize the 30S sites participating in the interactions with the 50S particle within the ribosome. Support for this presumed arrangement was provided recently, in a series of experiments in which DNA oligomers, complementary to several single-stranded segments of the 16S RNA, were diffused into T30S-HR crystals. We found that the infiltration of the oligonucleotide complementary to the 5′ end of the 16S RNA did not lead to any loss of crystal order. The oligomer that binds in solution to the decoding region [41,42], however, caused substantial disorder of the crystals in accordance with its location in the region involved in the pairing. It can also be a result of significant conformational changes caused by its binding.

The assumption that the T30S conformation selected by the HR crystals is close to that of active particles, led to the growth of both the HR and the LR crystals from particles trapped in their functionally active state (by chemical labeling and mild cross-linking during heat activation).

Figure 6

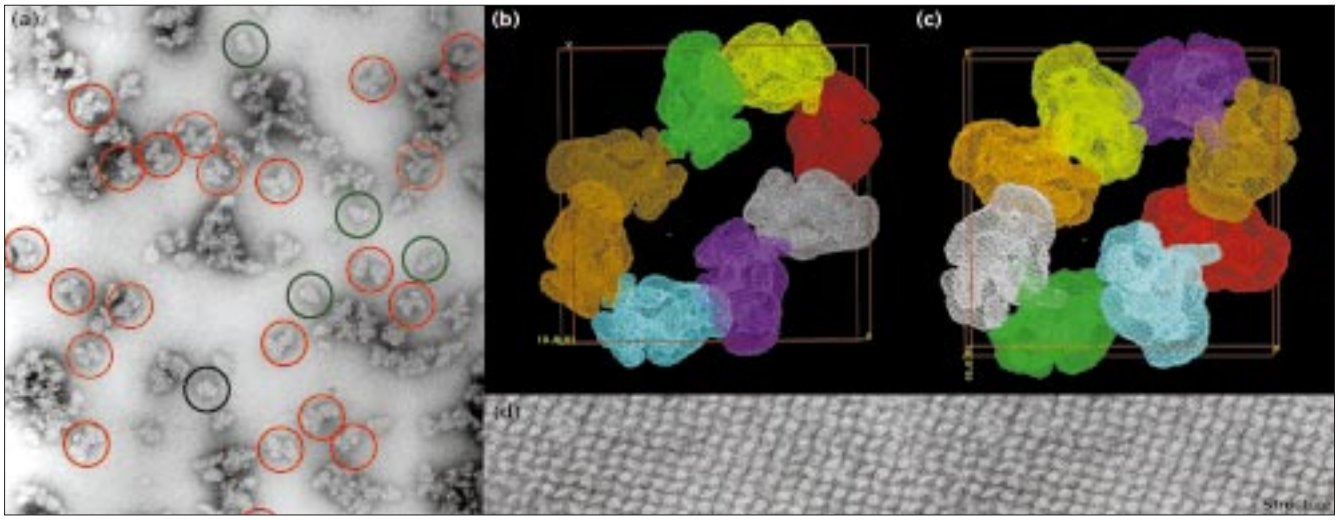

(a) A negatively stained preparation of carefully dissolved T30S-HR crystals observed by EM, showing the butterfly-like T30S pairs (in red circles) together with isolated particles (in green circles). The MR solutions, using the free T30S reconstruction with the X-ray amplitudes from (b) T30S-LR and (c) T30S-HR. (d) A negatively stained thin section of about 500 Å thickness, obtained from an epon-embedded T30S-LR crystal, in a direction approximately perpendicular to the c axis.

Figure 7

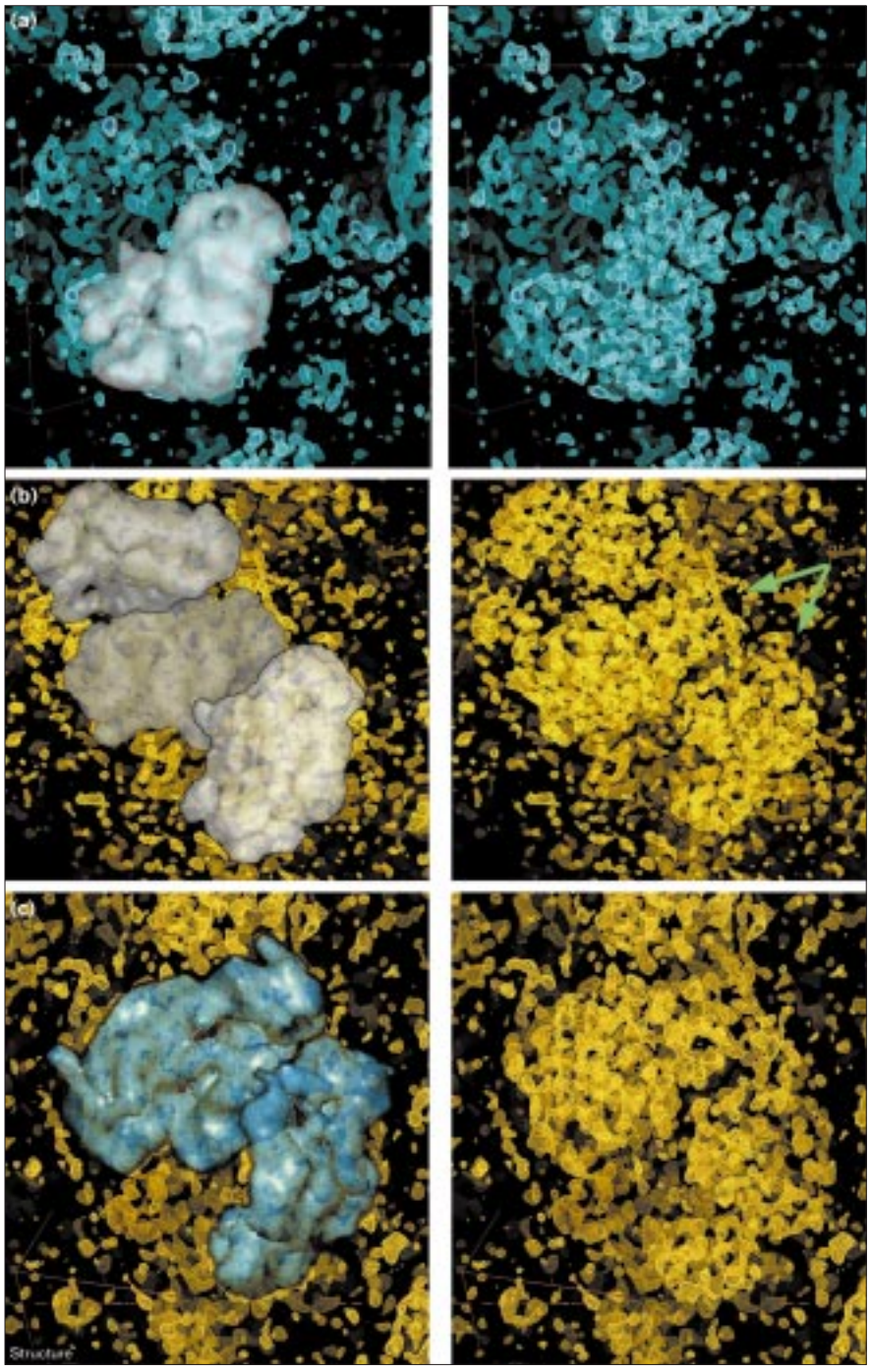

(a) The free T30S reconstruction overlaid on a part of the 7.2 Å MIR map. (b) Three reconstructions of the 'free' T30S overlaid on the 7.2 Å MIR map. The arrows point to the particles creating the extensive contact region (the crystallographic pair). The density between them belongs to a particle in a lower unit cell. (c) Two reconstructions of 'cut' T30S are overlaid on the 7.2 Å MIR map. The density between these originates partially from a particle belonging to a lower unit cell. In all, the right-hand panels show the corresponding part of the 7.2 Å map.

Interestingly, when using the LR crystallization conditions, the quality of these crystals grown from the trapped particles was much higher than that of the native ones, most probably because of their enhanced homogeneity. Furthermore, taking advantage of the sizeable internal solvent region within the crystal that would allow for significant conformational rearrangements, we heat-activated [43] the crystallized particles in order to increase the proportion of 30S particles in their active conformation. These experiments were performed on HR crystals that were found to yield moderate resolution, that is 5–6 Å instead of the expected 3–3.5 Å. Indeed, the controlled heating treatment led to a larger proportion of high quality crystals in our preparations and ensured that the main conformation studied by us is that of functionally active T30S particles.

Discussion

Several aspects of a fruitful interplay between cryo-EM three-dimensional reconstruction and X-ray crystallography are demonstrated in our studies of the *T. thermophilus* ribosome and its two subunits. The uniqueness of the MR solution for the T70S particle, along with the various verification tests, indicates that the resulting packing assembly (Figure 2) is correct. This result, by itself, does not add to the knowledge about the ribosome's structure, beyond what is already known from cryo-EM, but confirms independently the correctness of the cryo-EM three-dimensional reconstruction. Studies on the large subunits, T50S and H50S, have led to more meaningful structural results. Enhanced detail is expected for these particles given that the 17 Å EM reconstruction of T50S might be extended to higher resolution limits by incorporating phase information obtained independently by SIRAS. These studies also provide reliable tools for assessing the correlation between crystallographically determined phases and those obtained by MR, as well as for assessment of the level of the deviation from isomorphism.

Of special interest is the interplay between cryo-EM and crystallography of T30S that intersects several aspects of electron microscopy. The 7.2 Å map, in conjunction with the cryo-EM reconstructions, indicates that the conformation selected by the HR crystals is closed to that of the 30S particle within the assembled ribosome. It also shows pairing of the crystallized particles, an observation that was confirmed by negative-stain EM investigations of partially dissolved crystals. So far no functional relevance can be assigned to the crystallographic or to the previously observed induced pairing [43,44], but it is conceivable that the extensive interparticle interactions emulate some of the contacts in which the small subunit is involved at the intra-ribosomal subunit interface and/or the contacts needed for the formation of intermediates along the path of the translation cycle.

The solvent content of the ribosomal crystals falls within the range observed for other macromolecules (55–70%); the distribution of the solvent regions, however, is rather unique. Sizeable continuous solvent regions were detected in three out of the four crystal forms of the thermophilic ribosomal particles (all of space group $P4_12_12$) as well as in the form diffracting to the highest resolution, H50S, that has a different space group ($C222_1$). Interestingly, the lowest resolution crystals, those of T70S, show smaller solvent cavities, whereas an unusually large continuous solvent region, held rather loosely by one interparticle contact area, was found by MIRAS phasing in the crystals of H50S, the form diffracting to the highest resolution.

The usefulness of cryo-EM reconstructions in phasing data collected from crystals of large particles with no internal symmetry, such as the ribosomes, remains to be seen. Limiting factors stem from the weak diffraction power, the radiation sensitivity and the low level of isomorphism of the crystals, as well as from the character of the EM three-dimensional reconstruction. Thus, flexible particles are likely to yield reconstructions that represent the average of large spectrums of conformations that might differ from the conformation selected by the crystals and consequently might be of little help for MR phase determination. Complications, specific to low-resolution MR studies, arise from difficulties in the verification of the MR solutions. The powerful tool for assessing the reliability of the MR results, namely the correctness of bond lengths and bond angles, that emerges while refining high-resolution structures is missing at low resolution. Even parameters that are normally available for simpler macromolecular systems, such as their volume, bear uncertainties in the case of ribosomes. In addition, maps originating from MR phases lack information about a large fraction of the crystals, namely the non-crystalline solvent, because their structure factors are obtained by back Fourier transformation of the MR assembled map. At high resolution the solvent part of the structure factors might be negligible, but at low resolution (below 8–10 Å) the non-crystalline part might reach values similar to that of the crystalline material.

The H50S crystals pose a further problem because of the high electron density of the solvent, which reaches that of proteins [45], significantly reducing the contrast between the ribosomal proteins (which account for about 35% of the total particle mass) and the solvent. Consequently, in our 12 Å MIRAS map the RNA chains are readily detectable, whereas the outline of the surface ribosomal proteins is less well resolved [2]. Furthermore, it was found that the main differences between the MIRAS map of H50S and the MR solution are in the vicinity of the regions assigned as the locations of the external ribosomal proteins (Figure 4).

The MR searches performed for the verification of the X-ray results proved to be useful for the assessment of the level of structural heterogeneity, using their relative orientations as a guide. Although the orientation information — by itself — might be a rather poor indicator, when combined with the knowledge about the positions of the centers of mass, it was found to be quite useful. The ability (or inability) of the MR phases to reveal heavy-atom sites that were extracted independently by non-MR methods adds to the usefulness of the orientation information.

So far, only two of the large number of searches performed for H50S have yielded MR phases that confirmed heavy-atom sites at low resolutions [2,28]. As mentioned above, these are similar in position, but different in orientation. If indeed this shows two different conformers, it is conceivable that both will lead to structure determination. The

Ta_6Br_{14} site, revealed originally at approximately 10 Å by MIRAS [2], reconfirmed by MR, and shown to be stable at a relatively high resolution (i.e. about 5 Å) by anomalous crystallography, raises the expectations for further progress. The key for reliable structure analysis at high resolution, however, is increasing the level of isomorphism of the H50S crystals. We aim at reducing the conformational variability of the crystallized H50S particles by inducing controlled rearrangements within the crystals, along the lines found useful for the T30S crystals, namely by heat activation, or cross-linking prior to crystallization. The halophilic system poses a greater challenge in the design of such experiments, because of the high salt concentration in the crystallization solution.

Biological implications

Among all ribosomal particles that we examined, H50S and T30S yield the crystals diffracting to the highest resolution: 2.7 Å [1] and 3.0 Å [2], respectively. Whereas the crystals of H50S are highly non-isomorphous [2], we benefitted from the conformational variability of T30S in the growth of two crystal families (LR and HR), each exhibiting normal isomorphism. Consequently, an intermediate 7.2 Å multiple isomorphous replacement (MIR) map of T30S-HR was constructed, showing particles with elongated dense chains that were interpretable as rRNA, and regions fitting the size of average ribosomal proteins.

Cryo-EM reconstructions were found useful in assisting the X-ray crystallography of ribosomal particles and in highlighting several unusual aspects concerning their conformational variability. Thus, inspection of the T30S MIR map indicated that the conformation of the crystalline particles resembles that assigned to the small subunit within the reconstruction of T70S ribosomes. It is conceivable that part of the intensive interactions of T30S within the crystals (seen as pairs) exploits part of the high-affinity binding sites of T30S, such as those forming the interface between the small and large subunits within the assembled ribosome. Indeed, diffusion of DNA oligomers complementary to the 16S rRNA in the decoding region caused severe crystal damage. The destruction of the crystals suggests that the decoding region lies in the vicinity of the extensive interparticle contacts and can also indicate conformational changes that occur upon binding of this oligomer.

Following these observations, we were able to increase the number of crystals diffracting to around 3 Å from preparations showing somewhat lower quality (that is diffracting to 5–6 Å) by heat activation of the crystallized particles. We also obtained crystals of T30S that were chemically trapped in their activated state prior to crystallization and showed that the functionally active trapped particles are still sufficiently flexible to undergo further conformational changes within the crystal.

Finally, our studies are in agreement with the principle of ribosomal universality [13–17,19,45–47]. The MIRAS and MIR maps obtained by us for H50S and T30S show internal and external features revealed in ribosomes from other sources. Furthermore, we and others [28], have shown that the EM reconstructions of eubacterial ribosomal particles (E50S and T50S) are suitable for MR studies of ribosomes from archaea (H50S).

Materials and methods

Cryo-EM reconstruction

Ribosomes and subunits from the same preparations that gave the best three-dimensional crystals have been subjected to the cryo-EM and angular reconstruction procedures. Electron micrographs of the vitreous ice embedded specimens were taken in the liquid helium cooled microscope (SOPHIE) at a magnification of 66.000 and a defocus of about 0.9 microns. The Emil densitometer (Image Science GmbH, Berlin) was used to digitize the micrographs using a sampling step size of 14 μm. The pixel size was coarsened by a factor of 2 resulting in a sampling of 4.48 Å per pixel on the specimen scale. All image processing was performed with the IMAGIC-V software package [4]. Approximately 4000 individually boxed particles (of T30S, T50S and T70S) were aligned using an iterative multireference alignment (MRA) scheme. Upon subsequent application of multivariate statistical analysis (MSA) data compression and classification procedures, characteristic views of ribosomes could be obtained with improved signal-to-noise ratio. The Euler angles of these two-dimensional projection images were determined using the angular reconstruction approach [3].

The data set was submitted to several rounds of iterative refinement including retrojection of the three-dimensional reconstruction, MRA using reprojections as reference images, MSA/classification, Euler angle determination, and three-dimensional reconstruction as performed previously in the reconstruction of 70S from *E. coli* [7]. The resolution of the resulting three-dimensional reconstructions was determined using the Fourier Shell Correlation [48] function with a threshold value of 3σ. The differences in resolution obtained for the various samples can be explained mainly by their different degrees of conformational variability.

Crystal growth, X-ray data collection and MIR studies

The preparations of ribosomal particles, their crystallization and treatment were performed as described earlier [1,2,31,37] with minor modifications, associated mainly with mild treatment. Activation was achieved by heating [41]. For trapping the activated state, mild cross-linking was performed. Negatively stained, epon-embedded thin sections of three-dimensional crystals and negatively stained dissolved crystals were inspected using a Philips CM-100 as in [15,16]. Synchrotron radiation (SR) crystallographic data were collected at cryo-temperature and processed using the progams DENZO and SCALEPACK [49].

Data from the 70S complex crystals were collected at F1/CHESS (R_{merge} = 4.7% and completeness = 96% over the range 17–77 Å) and from T50S crystals at BW7b/EMBL/DESY. To exploit anomalous phase information, data from the Ta_6Br_{14} derivative were collected at two wavelengths: 1.2537 Å (LIII, maximum f″ peak) and 1.2547 Å (LIII near its inflection point, i.e. at maximum f′). The deviation from the Ta edge, namely 1.25530 Å, is caused by the chemical environment within the crystals and to the parameters of BW6/MPG/DESY, where these measurements were performed. Typical R_{merge} (for the three data sets) = 8.1% with completeness of 95–99%.

Data from T30S-LR crystal were collected at BW6/DESY (R_{merge} = 7.9%, completeness = 99.0% up to 12 Å), and from T30S-HR (and its derivatives) at F1/CHESS and ID2/ESRF. For the MR studies the shell up to 12 Å was used (R_{merge} = 6.2%, completeness = 99.6%).

For the construction of the 7.2 Å MIR map 20688 reflections in the range of 7.2–30 Å were included. The sites of the four derivatives were verified by difference Patterson and difference Fourier procedures (FOM = 0.671, phasing power up to 1.4, R_{cullis} = 0.8–0.91).

Data from 59 crystals of H50S, collected at several resolution ranges between 3 Å and 300 Å, were used for the MIRAS and MR studies reported here. These were collected at wavelengths 0.78–1.5 Å at the SR stations reported in the Acknowledgements section, on film, offline and online imaging-plate detectors or CCD cameras. The construction of the 12 Å MIRAS electron-density map is described in [2].

Molecular replacement

MR studies, exploiting cryo-EM three-dimensional reconstructions and SR data, rotation and translation searches, followed by rigid-body refinement, were performed using the program AMoRe [50]. The reconstructions were presented as envelopes of uniform density. Integration radii of lengths comparable to the assumed size of the ribosomal particles (i.e. 70–200 Å) were used. In order to resolve uncertainties between the X-ray and the cryo-EM data sets, the reconstructions were isotropically expanded or contracted by up to 20%, and each of the thus computed models was subjected to a full run of AMoRe. Several parameters, such as resolution shells and different integration radii, were fitted and optimized at each stage. The translation searches were performed for both enantiomorphic space groups, $P4_12_12$ and $P4_32_12$. A map of the unit-cell content was assembled by placing the optimized EM model according to the MR results followed by the application of the symmetry operations. Structure factors and phases were calculated by back transforming the MR assembled map (subroutine gendd in AmoRe). Agreement factors were computed by RSTATS and FOM by SIGMAA [51]. This test was not performed for T30S because neither of its MR results was fully satisfactory.

The searches for T70S were performed as follows. Rotations: 20–40, 20–50, 30–40, 20–34, 25–40 and 20–27 Å; integration radii 106–242 Å; translations: 20–40 and 20–60 Å; rigid-body refinement: 20–40, 20–60 and 20–80 Å; expansion/shrinkage = 0–20%. For T50S, rotation: 20–40, 17–35 and 18–67 Å; translation 20–40, 16–47 and 18–30 Å; rigid-body refinement 20–40 Å; integration radii = 113–133 Å; shrinkage 4%. For T30S, rotation: 25–40 Å; integration radii = 70–160 Å; translation and rigid-body refinement at 25–50 and 25–95 Å. For the 'free' model, optimal solution was obtained with 6% shrinkage (LR) and 0% (HR). No contraction/expansion was needed for the 'cut' T30S because it was obtained from optimized T70S and T50S. Over two dozen H50S data sets were searched, using rotation radii of 17–90 Å.

Acknowledgements

We are exceptionally grateful to the late HG Wittmann, with whom these studies were initiated. We thank M Safro for active participation in the phasing attempts, F Zemlin for the use the SOPHIE EM, W Preetz and M Pope for their generous gifts of heavy-atom compounds, W Traub for his constructive comments and A Podjarny for valuable suggestions. We also thank K Anagnostopoulos and H Avila for producing the cDNA oligomers and H Bartels, WS Bennett, H Hansen, D Janell, S Weinstein, M Peretz, M Piolleti, S Krumbholtz, T Auerbach, M Kessler, C Radzwill, R Albrecht, C Glotz, K Knaack, M Laschever, Y Halfon, S Meier, J Muessig and C Paulke for their participation in the different stages of these studies. Data were collected at EMBL and MPG beamlines at DESY; F1/CHESS, ID2,ID13,D2AM/ESRF, BL26/PF/KEK, and ID19/APS. Support was provided by the US National Institute of Health (NIH GM 34360), the German Ministry for Science and Technology (BMBF 05-641EA), the European Community (B104 CT 972188), BBSRC (28/SBD07611) and the Kimmelmann Center for Macromolecular Assembly at the Weizmann Institute. AY holds the Martin S Kimmel Professorial Chair.

References

1. von Boehlen, K., *et al.,* & Yonath, A. (1991). Characterisation and preliminary attempts for derivatisation of crystals of large ribosomal subunits from *Haloarcula marismortui*, diffracting to 3 Å resolution. *J. Mol. Biol.* 222,11-15.
2. Yonath, A., *et al.,* & Franceschi, F. (1998). The quest for the molecular structure of a large macromolecular assembly exhibiting severe non-isomorphism, extreme beam sensitivity and no internal symmetry. *Acta Crystallogr. A* 54, 945-955.
3. van Heel, M. (1987). Angular reconstitution: *a posteriori* assignment of projection directions for 3D reconstructions. *Ultramicroscopy* 21, 111-124.
4. van Heel, M., Harauz, G. & Orlova, E. (1996). A new generation of the IMAGIC image processing system (Image Science GmbH Berlin). *J. Struct. Biol.* 116, 17-24.
5. Radermacher, M., Wagenknecht, T., Verschoor, A. & Frank, J. (1987). Three-dimensional reconstruction from single-exposure, random conical tilt series applied to the 50S ribosomal subunit. *J. Microscopy* 146, 113-136.
6. Frank, J. (1996). *Three-Dimensional Electron Microscopy of Macromolecular Assemblies.* Academic Press, San Diego.
7. Stark H., *et al.,* & van Heel M. (1995). The 70S *E. coli* ribosome at 23 Å resolution: fitting the ribosomal RNA. *Structure* 3, 815-821.
8. Frank, F., *et al.,* & Agrawal, R.K. (1995). A model of protein synthesis based on cryo electron microscopy of the *E. coli* ribosome. *Nature* 376, 441-444.
9. Agrawal, K.R., Penczek, P., Grassucci, R.A., Li, Y., Leith, A.D., Nierhaus, K.H & Frank, J. (1996). Direct visualization of A-, P- and E-site tRNA in the *E. coli* ribosome. *Science* 271, 1000-1002.
10. Stark, H., *et al.,* & van Heel, M. (1997). Arrangement of the tRNAs in pre- and post translational ribosomes revealed by electron cryo-microscopy. *Cell* 88, 19-28.
11. Stark, H., Rodina, M.V., Rinke-Appel, J., Brimacombe, R., Wintermeyer, W. & van Heel, M. (1997). Visualization of elongation factor Tu in the *E. coli* ribosomes. *Nature* 389, 403-406.
12. Agrawal, K.R., Penczek, P., Grassucci, R.A. & Frank, J. (1998). Visualization of the elongation factor G on *E. coli* 70S ribosome: the mechanism of translation. *Proc. Natl Acad. Sci. USA* 95, 6134-6138.
13. Malhotra, A., *et al.*, & Frank, J. (1998). *E. coli* 70S ribosome at 15 Å resolution by cryo-electron microscopy: localization of fMet-$tRNA_f^{Met}$ and fitting of L1 protein. *J. Mol. Biol.* 280, 103-115.
14. Milligan, R. & Unwin, P.N.T. (1986). Location of the exit channel for nascent proteins in 80S ribosomes. *Nature* 319, 693-696.
15. Yonath, A., Leonard, K.R. & Wittmann H.G. (1987). A tunnel in the large ribosomal subunit revealed by three-dimensional image reconstruction. *Science* 236, 813-816.
16. Arad, T., Piefke, J., Weinstein, S., Gewitz, H.S., Yonath, A. & Wittmann, H.G. (1987). Three-dimensional image reconstruction from ordered arrays of 70S ribosomes. *Biochimie* 69, 1001-1006.
17. Yonath, A. & Berkovitch-Yellin, Z. (1993). Hollows, voids, gaps and tunnels in the ribosome. *Curr. Opin. in Struct. Biol.* 3, 175-180.
18. Berkovitch-Yellin, Z., Bennett, W.S. Yonath, A. (1992). Aspects in structural studies on ribosomes. *CRC Rev. Biochem. Mol. Biol.* 27, 403-444.
19. Yonath, A. & Franceschi, F. (1998). Functional universality and evolutionary diversity: insights from the structure of the ribosome. *Structure* 6, 678-684.
20. Berkovitch-Yellin, Z., Wittmann, H.G. & Yonath, A. (1990). Low resolution models for ribosomal particles reconstructed from electron micrographs of tilted two-dimensional sheets: tentative assignments of functional sites. *Acta Crystallogr. B* 46, 637-644.
21. Jack, A. Harrison, S.C. & Crowther, R.A. (1975). Structure of tomato bushy stunt virus: comparison of results obtained by EM and X-ray diffraction. *J. Mol. Biol.* 97, 163-172.
22. Rossmann, M.G. (1995). *Ab initio* phase determination and phase extension using non-crystallographic symmetry. *Curr. Opin. Struct. Biol.* 5, 650-655.
23. Urzhumtzev, A., Podjarny, A. (1995). On the solution of the molecular replacement problem at very low resolution: application to large complexes. *Acta Crystallogr. D* 51, 888-895.
24. Loewe, J., Stock, D., Jap, B., Zwickl, P., Baumeister, W. & Huber, R. (1995). Crystal structure of the 20S proteosome from Archeon *T. acidophilum* at 3.4 Å resolution. *Science* 268, 533-539.
25. Braig, K., Otwinowski, Z., Hedge, R., Boisvert, D.C., Joachimiak, A., Horwich, A.L. & Sigler, P.B. (1994). The crystal structure of the bacterial chaperonin at 2.8 Å. *Nature* 371, 578-582.
26. Luger, K., Maeder, A.W., Richmond R.K., Segent, D.F. & Richmond, T.J. (1997). Crystal structure of the nucleosome core particle at 2.8 Å resolution. *Nature* 389, 251-260.
27. Rayment, I., Holder, H., Whittaker, M., Yohn, C., Lorenz, M., Holmes, K. & Milligan, R. (1993). Structure of the actin-myosin complex and its implications for muscle contraction. *Science* 261, 58-65.

28. Ban, N., *et al.*, & Steitz, T. (1998). The 9 Å resolution X-ray crystallography map of the large ribosomal subunits. *Cell* **93**, 1105-1115.
29. Trakhanov, S.D., *et al.*, & Moras, D. (1989). Preliminary X-ray investigation on 70S ribosome crystals. *J. Mol. Biol.* **209**, 327-334.
30. Berkovitch-Yellin Z., *et al.*, & Wittmann H.G. (1991). Crystals of 70S ribosomes from thermophilic bacteria are suitable for X-ray analysis at low resolution. *J. Crystal Growth* **110**, 208-213.
31. Hansen, H.A.S., *et al.*, & Yonath, A. (1990). Crystals of complexes mimicking protein biosynthesis are suitable for crystallographic studies. *Biochem. Biophs. Acta* **1050**, 1-5.
32. Volkmann, N., *et al.*, & Wittmann, H.G. (1990). Characterization and preliminary crystallographic studies on large ribosomal subunits from *Thermus thermophilus*. *J. Mol. Biol.* **216**, 239-243.
33. Dude, P., *et al.*, & van Heel, M. (1998). The 80S rat liver ribosome at 25 Å resolution by electron microscopy and angular reconstruction. *Structure* **6**, 398-399.
34. Franceschi, F. *et al.*, & Yonath, A. (1994). Crystallography, biochemical and genetics studies on halophilic ribosomes. *Syst. Apl. Microbiol.* **16**, 197-205.
35. Roth, M., *et al.*, & Yonath, A. (1996). On low resolution phasing of neutron diffraction data collected from ribosomal crystals. In *Biological Structure and Dynamics.* Proceedings of the 9th Conversation (R.H. Sarma and M.H. Sarma eds.), pp. 15-24, Adenine Press, NY.
36. Lata A.R, Agrawal, R.K., Penczek, P., Grassucci, R., Zhu, J. & Frank, J. (1996). Three-dimensional reconstruction of the *E. coli* 30S ribosomal in ice. *J. Mol. Biol.* **262**, 43-52.
37. Franceschi, F., *et al.*, & Yonath, A. (1993). Towards atomic resolution of prokaryotic ribosomes: crystallographic, genetic and biochemical studies. In *The Translational Apparatus* (K. Nierhaus ed.), pp. 397-410, Plenum Press, NY.
38. Yonath, A. Glotz, C. Gewitz, H.S. Bartels, K. von Boehlen, K. Makowski, I. & Wittmann, H.G. (1988). Characterization of crystals of small ribosomal subunits. *J. Mol. Biol.* **203**, 831-833.
39. Schluenzen F., *et al.*, & Yonath A. (1995). A milestone in ribosomal crystallography: the construction of preliminary electron density maps at intermediate resolution. *J. Biochem. Cell Biol.* **73**, 739-749.
40. Richmond, T.J., Finch, J.T., Rushton, B., Rhodes, D., & Klug, A. (1984). Structure of the nucleosome core particle at 7 Å resolution. *Nature* **311**, 532-537.
41. Weller, J.W., & Hill, W.E. (1992). Probing dynamic changes in rRNA conformation in the 30S subunit of the *E. coli* ribosome. *Biochemistry* **31**, 2748-2757.
42. Oakes, M.I., Clark, M.W., Henderson, E. & Lake, J.A., (1986). DNA hybridization electron microscopy: ribosomal RNA nucleotides 1392-1407 are exposed in the cleft of the small subunit. *Proc. Natl Acad. Sci. USA* **83**, 275-279.
43. Zamir A., Miskin, R. & Elson, D.(1971). Inactivation and reactivation of ribosomal subunits: amino acyl-transfer RNA binding activity of the 30S subunits of *E. coli*. *J. Mol. Biol.* **60**, 347-364.
44. Guerin M.F. & Hayes, D.H. (1987). Comparison of active and inactive forms of the *E. coli* 30S ribosomal subunits. *Biochemie* **69**, 965-974.
45. Anderson, K.M. & Hovmoeller, S. (1988). The average atomic volume and density of protein. *Z. Kristallogr.* **213**, 369-373.
46. Verschoor A., Warner JR. Srivastava S. Grassucci RA. Frank J. (1998). Three dimensional structure of the yeast ribosome. *Nuc Acids Res.* **26**, 655-661.
47. Verschoor, A. Srivastava, S., Grassucci, R. & Frank (1996). Native 3D structure of eukaryotic 80S ribosome: morphological homology with the *E. coli* 70S ribosome. *J. Cell. Biol.* **133**, 495-505.
48. Harauz, G. & van Heel, M. (1986). Exact filters for general geometry three-dimensional reconstruction. *Optik* **73**, 146-156.
49. Otwinowski, Z. (1993). Data collection and processing. In *Proceedings of CCP4 Study Weekend*. p.p. 56-62.
50. Navaza J. (1994). AMoRe: an automated package for molecular replacement. *Acta Crystallogr. A* **50**, 57-163.
51. Collaborative Computational Project, No. 4 (1994). The CCP4 suite: programs for protein crystallography. *Acta Crystallogr. D* **50**, 760-763.

Because *Structure with Folding & Design* operates a 'Continuous Publication System' for Research Papers, this paper has been published on the internet before being printed (accessed from http://biomednet.com/cbiology/str). For further information, see the explanation on the contents page.